Alpha radiation effects on silicon oxynitride waveguides

Francesco Morichetti[1*], Stefano Grillanda[1], Sandeep Manandhar[2], Vaithiyalingam Shutthanandan[2], Lionel Kimerling[3], Andrea Melloni[1], and Anuradha M. Agarwal[4]

[1]*Politecnico di Milano, Dipartimento di Elettronica, Informazione e Bioingegneria, 20133 Milano, Italy*
[2]*EMSL, Pacific Northwest National Laboratory, Richland, Washington 99352, USA*
[3]*Massachusetts Institute of Technology, Department of Materials Science and Engineering, Cambridge, Massachusetts 02139, USA*
[4]*Massachusetts Institute of Technology, Materials Processing Center, Cambridge, Massachusetts 02139, USA*

Abstract: Photonic technologies are today of great interest for use in harsh environments, such as outer space, where they can potentially replace current communication systems based on radiofrequency components. However, akin to electronic devices, the behavior of optical materials and circuits can be strongly altered by high-energy and high-dose ionizing radiation. Here, we investigate the effects of alpha (α) radiation with MeV-range energy on silicon oxynitride (SiON) optical waveguides. Irradiation with a dose of 5×10^{15} cm^{-2} increases the refractive index of the SiON core by nearly 10^{-2}, twice as much as that of the surrounding silica cladding, leading to a significant increase of the refractive index contrast of the waveguide. The higher mode confinement induced by α-radiation reduces the loss of tightly bent waveguides. We show that this increases the quality factor of microring resonators by 20%, with values larger than 10^5 after irradiation.

Keywords: Integrated photonics, high-energy radiations, silicon-oxynitride waveguides, alpha particles

TOC Graphic
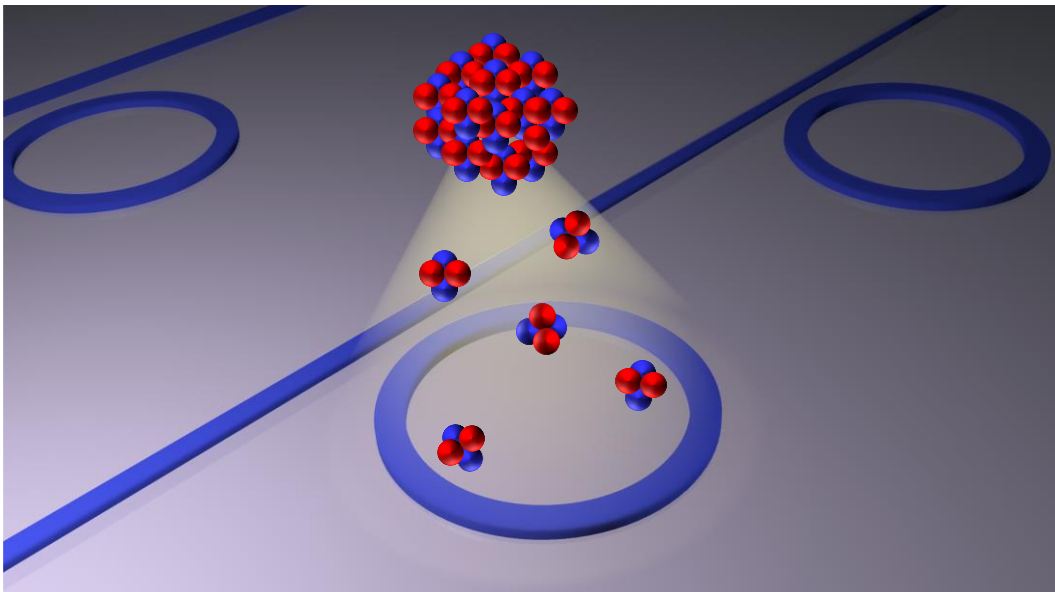
High-levels of ionizing radiation may be responsible for damage and fault events in devices working in harsh environments, such as outer space, or near nuclear reactors and particle accelerators [1]. Most semiconductor electronic components are sensitive to high-energy particles that can cause soft errors, like data flip in memory cells and registers [2], or even destructive effects in high-power transistors. Radiation sources can also be hidden in some parts of the component itself: for instance, alpha (α) particles emitted by impurities in packaging materials were shown to be the main cause of soft errors in dynamic random-access memories and charge-coupled devices [3]. Several radiation-hardening techniques have been developed to ensure robust operation of integrated electronic systems in harsh environments.

More recently, the exploitation of optical technologies [4-7], and especially of photonic integrated circuits [4-5], in harsh environments has attracted the interest of space agencies. In addition to the traditional use of optics in space to make imaging systems or reflectors, integrated photonics is believed to have the potential to revolutionize current space communication systems, based on radiofrequency components, with smaller, lighter and higher transmission capacity devices [4-7]. Therefore, understanding the effects of high-energy radiation on photonic components is now of primary importance. To date most research in the field has addressed the impact of radiations on optical fibers [8] and bulk optical materials [9-10] only, and very few have investigated the effects on photonic integrated circuits [11-17], primarily based on silicon [11-13], silicon nitride [14], lithium niobate [15] and polymer materials [11,16-17]. Further, no studies have reported the effects of high-energy α-radiations, consisting of two protons and two neutrons bound together as in a helium nucleus, on photonic integrated waveguides or circuits.

Here, we experimentally investigate the effects of α-radiations on silicon oxynitride (SiON) photonic integrated circuits. We consider different devices, such as Mach-Zehnder

interferometers (MZIs) and microring resonators (MRRs), to show how radiations affect the behavior of the optical waveguide and of different photonic circuits. As a main effect, we find that after exposure to α-rays with energy in the MeV-range, SiON waveguides experience a significant increase of the refractive index contrast Δn, which is due to a larger change of the SiON core refractive index compared to that of the silicon dioxide (SiO$_2$) cladding. The higher mode confinement induced by radiations strongly reduces the loss of tightly bent waveguides, leading to a significant increase of the quality factor of MRRs, with values exceeding 10^5 after irradiation.

Figure 1(a) shows a schematic view of the waveguides considered in this work. The SiON core, with refractive index 1.513 at 1550 nm, is deposited by means of plasma enhanced chemical vapor deposition and has a square cross-section of size 2.2 μm × 2.2 μm. The core is surrounded by a SiO$_2$ cladding with refractive index 1.4456, with a thickness of 15 μm below the SiON core and 7 μm on top of it. The refractive index contrast Δn of the as-fabricated waveguide is 4.45%. Propagation loss is 0.25 dB/cm, as discussed in [18], where more details on the waveguide fabrication technology and characterization can be found.

The samples hosting the SiON devices were entirely and uniformly exposed to α-radiation with energy of 2.3 MeV. The energy of irradiation was chosen to induce most of the damage in the center of the SiON core of the waveguides, where the optical mode has its maximum intensity, thus maximizing the impact of radiation on the fabricated circuits. Figure 1(b) shows a simulation, performed with the SRIM/TRIM software [19], of the damage distribution induced by the penetration of helium ions with 2.3-MeV-energy into the materials stack of Fig. 1(a). In particular, considering that in our experiments we employ an ion dose in the range between 10^{15} cm^{-2} and 5×10^{15} cm^{-2}, a peak damage density in the range between 0.9×10^{21} cm^{-3} and 4.5×10^{21} cm^{-3} is induced in the center of the SiON core. If α-particles with energy lower than 2 MeV or higher than
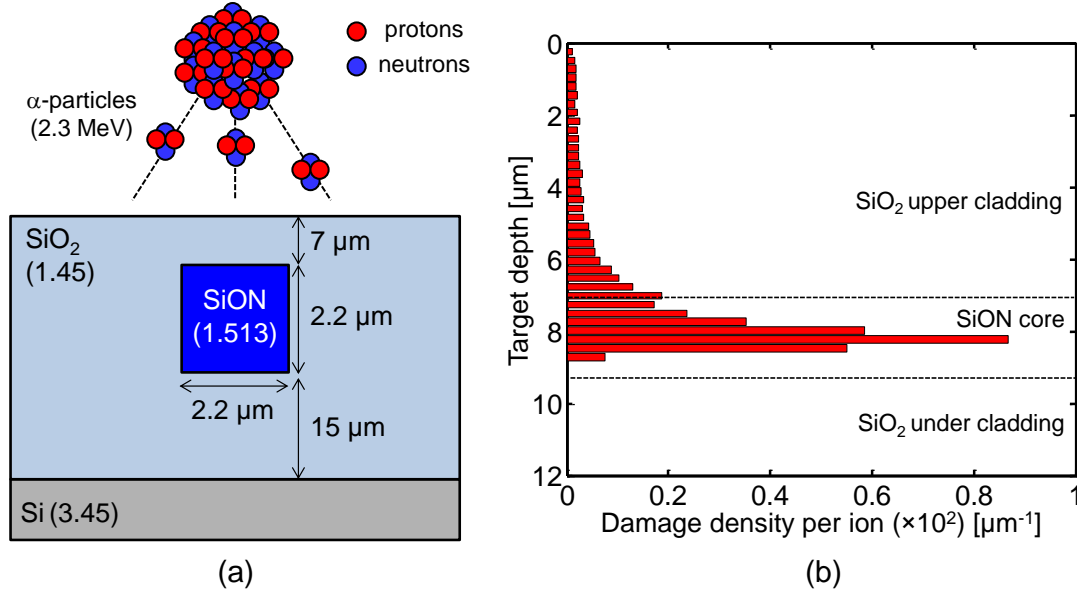
Fig. 1. Exposure of SiON waveguides to α-radiation. (a) Schematic of the waveguide cross-section. (b) Simulation of the damage distribution induced by α-particles versus the penetration depth in the materials stack of Fig. 1(a). An energy of 2.3 MeV induces the maximum damage at the level of the SiON core of the waveguide.

2.5 MeV were used, the peak of the damage distribution would shift respectively into the upper or lower cladding of the waveguide (see Supporting Note 1), thus having less impact on the waveguide behavior.

To evaluate the effects of α-rays on photonic devices, we first consider the case of an unbalanced MZI exposed to a dose of 10^{15} cm^{-2} [Fig. 2(a)]. Figure 2(b) reports the measured transfer function at the bar port of the MZI on transverse-electric (TE) polarization before (blue dashed curve) and after (red solid curve) irradiation. Due to the low polarization sensitivity of the waveguide, a similar behavior was observed on transverse-magnetic (TM) polarization. The 500 μm unbalance ΔL between the MZI arms translates into a free-spectral-range FSR of 3.145 nm (391.33 GHz). The exposure to radiations does not appreciably change the shape or extinction ratio (ER) of the MZI response. This suggests that, at this dose, neither the propagation loss of the waveguides nor the coupling ratio K of the 3 dB directional couplers has changed. In this device,

the bending loss is not relevant, since the waveguides are weakly bent (1200 μm radius) compared to the minimum radius (300 μm) at which bending loss becomes significant.

A rigid wavelength shift $\Delta\lambda$ of the MZI transfer function is observed, together with a tiny reduction of the *FSR*. After exposure, the *FSR* decreases by about 15 pm, indicating that the waveguide group index $n_g = c/(FSR\times\Delta L) = 1.534$ increases by about $\Delta n_g = (\Delta FSR/FSR)n_g = 7\times10^{-3}$. As the temperature of the chip is controlled by a thermo-electric cooler within 0.1°C (that means with a 1 pm wavelength stability of the MZI response), the measured wavelength shift has to be attributed to a radiation-induced change of the waveguide effective index Δn_{eff}. To quantify $\Delta\lambda$ with no ambiguity due to the periodicity of the MZI spectrum, electromagnetic simulations performed through the beam propagation method (BPM) where carried out to relate Δn_g and Δn_{eff} of the SiON waveguide to the variation of the refractive index of the SiON core and of the SiO_2 cladding. According to the results reported in Fig. 2(c), the measured Δn_g of 7×10^{-3} (solid line) is consistent with different values of Δn_{eff} (dashed lines), each one corresponding to a wavelength shift of the MZI response by an increasing number of *FSRs*. Among the possible solutions indicated in the map (circles), only the case $\Delta n_{eff} = 5.2\times10^{-3}$ (corresponding to $\Delta\lambda = 5.3$ nm) is associated with an increase of the waveguide index contrast Δn (white region of the map), while all the other solutions would imply a decrease of Δn (gray region). As we will fully justify in the remainder of this paper, exposure to α-rays leads to an increase of the SiON waveguide index contrast. Therefore, we can conclude that a dose of 10^{15} cm^{-2} is responsible for a change of the refractive index of the SiO_2 cladding and of the SiON core by 2.65×10^{-3} and 5.9×10^{-3}, respectively (red circle in the white region of the map).
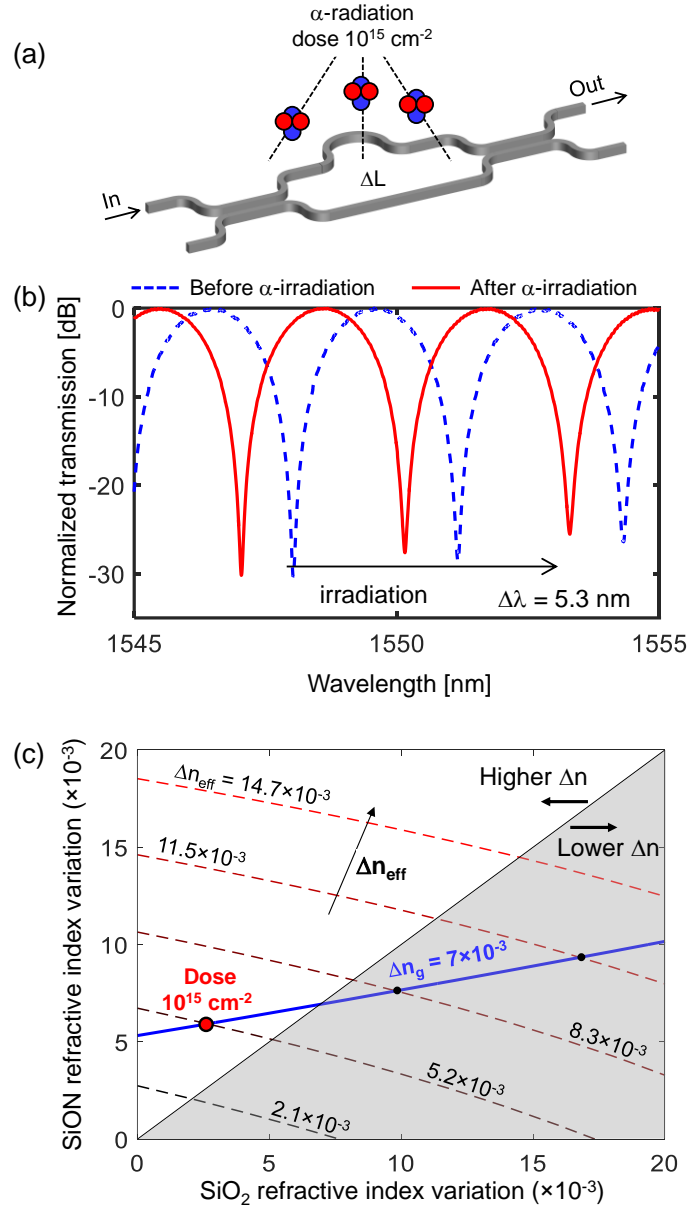
Fig. 2. (a) Schematic of a MZI irradiated with α-radiation. (b) Normalized transmission of the MZI before (dashed blue curve) and after (solid red curve) exposure to a dose of 10^{15} cm^{-2}. (c) Simulated variation of the effective index variation Δn_{eff} (dashed lines) of the SiON waveguide versus the variation of the refractive index of the SiON core and of the SiO$_2$ cladding. The blue solid line shows the points where Δn_g matches the measured value of $\Delta n_g = 7 \times 10^{-3}$. White/gray regions indicate an increase/decrease of the refractive index contrast of the waveguide, respectively. The red circle shows the measured change of the MZI waveguide after exposure to α-rays.

To get a deeper insight into the effects of α-radiation on the SiON platform, further experiments were carried out on MRRs exposed to a radiation dose of 5×10^{15} cm^{-2}, that is $5\times$ larger than the irradiated MZI of Fig. 2. Several MRR all-pass filters with a racetrack shape as in the sketch of Fig. 3(a) were fabricated, with a round-trip geometric length $L = 1955.3$ μm and $FSR = 800$ pm (99.9 GHz). Different coupling ratios K, from 0.05 to 0.8, between the MRR and the bus waveguide are obtained by keeping the same gap distance (1.8 μm) between the coupled waveguide, and by increasing the coupling length L_c (from 30 μm to 315 μm), thus implying a reduction of the bending radius R (from about 300 μm to 210 μm) for higher K.

Figure 3(b) shows the TE-polarized transfer function of a MRR before (blue dashed curve) and after (red solid curve) α-ray exposure across a 60 nm wavelength range. The MRR has nominal power coupling ratio $K = 0.5$, -3 dB bandwidth of 165 pm (20.6 GHz) and quality factor Q of 9.4×10^3. Figures 3(c)-(d)-(e) show a detailed view of the resonator response before and after irradiation at the edges (1520 nm and 1580 nm) and in the center (1550 nm) of the considered wavelength range. Based on the comparison of the mutual wavelength position of the MRR resonances, it is confirmed the reduction of the FSR occurs under the effect of α-rays, here amounting to about 24 pm, and corresponding to $\Delta n_g = 1.16\times10^{-2}$. A similar behavior was observed on TM polarization as well, where the measured Δn_g is 1.17×10^{-2}. After irradiation, the MRR spectrum also exhibits a significant ER reduction: for instance, at wavelength around 1579 nm [Fig. 3(e)], the ER reduces from more than 23 dB (blue) to about 17 dB (red).
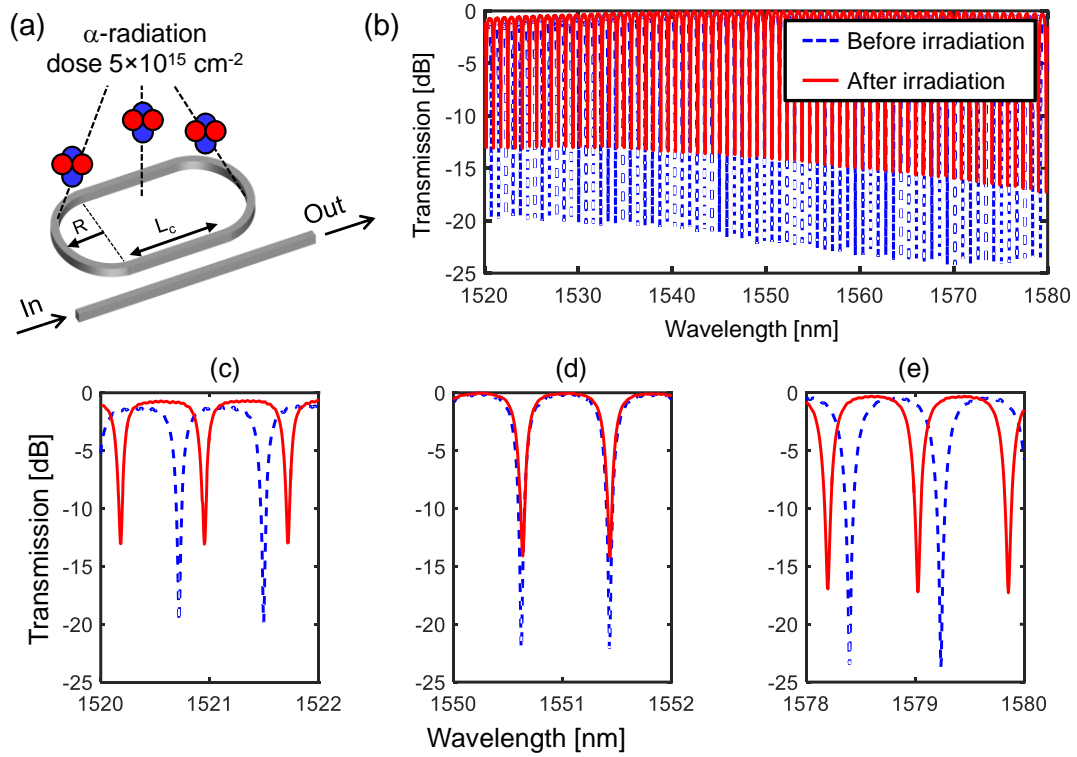
Fig. 3. (a) Exposure of a MRR to α-radiation with a dose of $5 \cdot 10^{15}$ cm^{-2}. Transfer function of the resonator before (blue dashed curve) and after (red solid curve) irradiation (b) across a wavelength range of 60 nm and (c-d-e) detailed view at the edges and in the center of the considered spectrum.

A systematic characterization of all the fabricated MRRs is reported in Figs. 4-5, providing a comprehensive picture of the irradiation-induced changes of the optical parameters of SiON MRRs. The more evident result is that α-radiation significantly increased the Q-factor of all the MRRs. As shown in Fig. 4(a), before irradiation (blue squares) the Q-factor of the as-fabricated MRRs ranges from 4.6×10^3 ($K = 0.8$) to 9.5×10^4 ($K = 0.05$). After irradiation (red circles) an average increase of the Q-factor by about 20% (with 5% standard deviation among the different MRRs) is observed. The normalized spectra of the MRRs before and after irradiation are reported in the insets of the figure. Figure 4(b) also shows that after exposure the ER of all the MRRs has reduced; in particular, the largest ER variation is experienced by the MRRs with K around 0.5, that
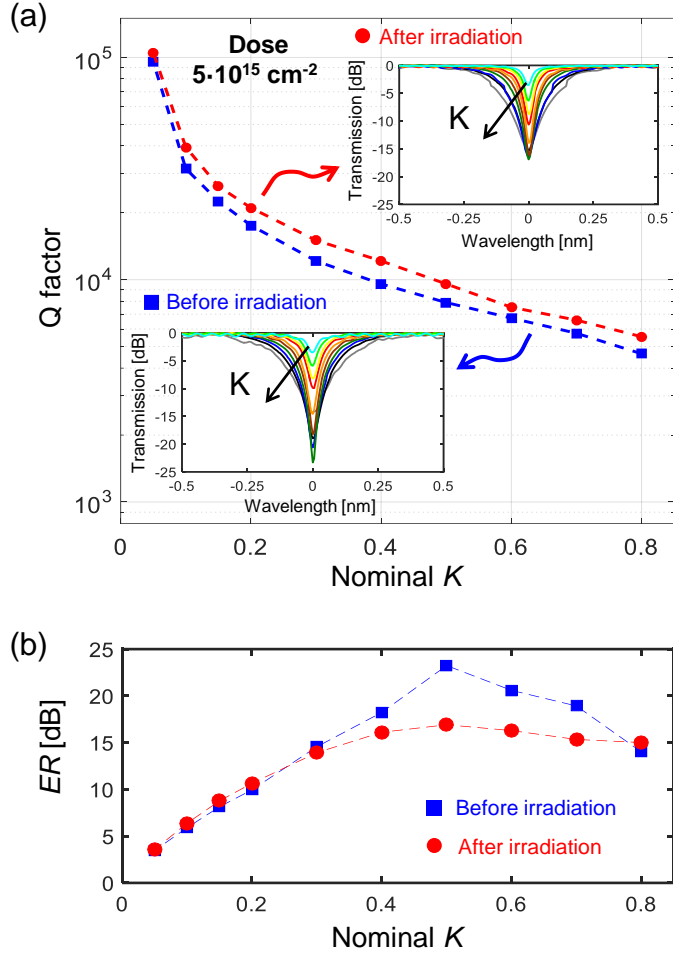
Fig. 4. Effect of α-radiation on (a) the *Q*-factor and (b) the *ER* of SiON MRRs, with same length as that of Fig. 3 but with coupling coefficients *K* ranging from 0.05 to 0.8, before (blue squares) and after (red circles) exposure to α-radiation with 5×10^{15} cm^{-2} dose. The MRR transfer functions around 1580 nm are shown in the insets.

operate near the critical coupling condition, while for MRRs with higher *Q*-factors (*K* < 0.3), almost no change in the *ER* is observed.

In principle, an increase of the *Q*-factor can originate from either a reduction of the round trip loss or a reduction of the coupling ratio *K*. To extract the optical parameters of the SiON waveguide before and after irradiation, all the MRR spectra were numerically fitted as shown in the Supporting Note 2. Figures 5(a)-(b) show the values of the coupling ratios and round trip loss extracted from the numerical fit, before (blue squares) and after (red circles) irradiation. Results

10

indicate that irradiation with a dose of 5×10^{15} cm^{-2} causes a significant decrease of both K and round trip loss for every MRR. This behavior is consistent with a higher confinement of the optical field in the waveguide core, that is with an increase of the refractive index contrast Δn. Therefore, in Fig. 5(c), as well as for the MZI of Fig. 2(c), we can exclude the gray area of the map, where a decreasing Δn is implied. Considering also that MRRs have been exposed to a higher dose compared to the MZI experiment [reported for clarity also in Fig. 5(c)] a higher change of the materials refractive indices is expected. To discriminate among the four possible solutions indicated by circles in the map of Fig. 5(c), corresponding to different variation of the index contrast Δn, we exploited the information on the reduction of the coupling ratio K of Fig. 5(a). BPM simulations were carried out to evaluate the impact of core/cladding refractive index variations on the behavior of the as-fabricated directional couplers [blue dashed line, Fig. 5(a)]. Numerical results [red dotted line, Fig. 5(a)] indicate that the measured reduction of the coupling ratio K is in line with a change of the refractive index of the SiO$_2$ cladding and of the SiON core by 4.6×10^{-3} and 9.9×10^{-3}, respectively [red circle in the map of Fig. 5(a)] (see Supporting Note 3 for details). The related change of the waveguide effective index ($\Delta n_{eff} = 8.74\times10^{-3}$) implies that the response of the MRRs has shifted by 8.83 nm, that is about 11 *FSRs*, as indicated by the dashed lines in Fig. 5(c). Even though the refractive index change is not linear with the α-ray dose ($5\times$ dose causes a $2\times$ index variation), the twofold variation of the SiON index compared to the SiO$_2$ index change is preserved with the higher dose.
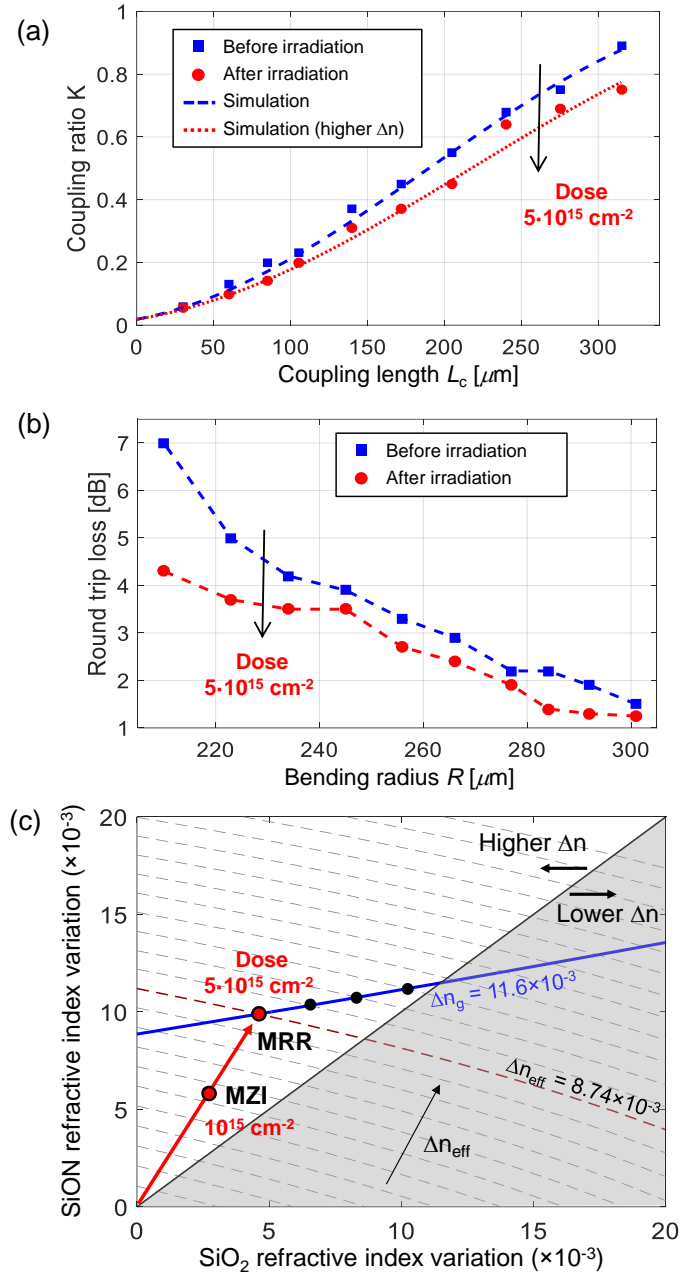
Fig. 5. Variation of (a) coupling ratio K and (b) round trip loss of the MRRs before (blue squares) and after (red circles) exposure to a dose of 5×10^{15} cm^{-2}. (c) Simulated Δn_{eff} (dashed lines) of the SiON waveguide versus the variation of the refractive index of the SiON core and of the SiO$_2$ cladding. The blue solid line shows the measured value of $\Delta n_g = 1.16 \times 10^{-2}$ for the MRRs. White/gray regions indicate an increase/decrease of the refractive index contrast of the waveguide, respectively. The red circles show the measured change of the waveguides after exposure to α-rays.

Table 1. Variation of the SiO$_2$ and SiON refractive indices as a function of the α-ray dose (energy is 2.3 MeV).

Dose [cm^{-2}]	SiO$_2$ index variation	SiON index variation	Index contrast Δn [%]
0	-	-	4.45
1×10^{15}	2.65×10^{-3}	5.9×10^{-3}	4.65
5×10^{15}	4.6×10^{-3}	9.9×10^{-3}	4.8

In conclusion, we have reported on an extensive investigation of the effects of α-radiation with MeV-energy on the behavior of SiON waveguides with an index contrast of 4.45%. As summarized in Table 1, the SiON core material experiences a change of refractive index that is more than 2× larger that of the surrounding SiO$_2$ cladding. This leads to an increase of the waveguide index contrast Δn from 4.45% to about 4.8% after irradiation with a dose of 5×10^{15} cm^{-2}. At this dose, α-radiations are also responsible for a wavelength shift of the transfer function of interferometric devices, such as MZIs and MRRs, by nearly 10 nm. No appreciable change of the waveguide propagation loss is associated with the refractive index variation. In contrast, a reduction in the loss of tightly bent waveguides and in the coupling ratio of directional couplers is observed. Both effects lead to a strong increase in the quality factor of MRRs (by about 20%), with values higher than 10^5 after exposure to α-particles. Therefore, despite the radiation-hard behavior of the waveguide loss, the strong sensitivity of the refractive index makes SiON interferometric circuits vulnerable to α-particles with high-dose and high energy. This also suggests the potential use of this optical technology as a sensor or dosimeter for this type of radiation.

Supporting Information Available. SRIM/TRIM simulations with α-particles with different energy; details on the numerical fit of the microring resonators spectra; numerical analysis of the directional couplers. The Supporting Information is available free of charge on the ACS Publications website at DOI:10.1021/acsphotonics.XXXXXXX.

Author Information

(*)Corresponding Author: francesco.morichetti@polimi.it

F. Morichetti and S. Grillanda equally contributed to this work.

The Authors declare no competing financial interest.

References

1) Holmes-Siedle, A. G.; Adams, L. Handbook of Radiation Effects (Oxford University Press, England 2002). ISBN 0-19-850733-X

2) Baumann, R. C.; Radiation-induced soft errors in advanced semiconductor technologies. *IEEE Trans. on Device and Materials Reliability* **2005**, 5(3), 305-316.

3) May T. C.; Woods, M. H. Alpha-particle-induced soft errors in dynamic memories. *IEEE Trans. on Electron Devices* **1979**, 26(1), 2-9.

4) Cornwell, D. Space-Based Laser Communications Break Threshold. *Optics & Photonics News* **2016**, 27 (5), 24-31.

5) NASA (2016). NASA engineers tapped to build first integrated-photonics modem. http://www.nasa.gov/feature/goddard/2016/nasa-engineers-tapped-to-build-first-integrated-photonics-modem.

6) Hemmati, H. Interplanetary Laser Communications. *Optics & Photonics News* **2007**, 18(11), 22-27.

7) Karafolas, N.; Armengol, J. M. P.; Mckenzie, I. Introducing photonics in spacecraft engineering: ESA's strategic approach. *IEEE Aerospace conference 2009, p.15.*

8) Gusarov, I.; Berghmans, F.; Deparis, O.; Fernandez Fernandez, A.; Defosse, Y.; Mégret, P.; Décreton, M.; Blondel, M. High total dose radiation effects on temperature sensing fiber Bragg gratings. *IEEE Photon. Technol. Lett.* **1999**, 11 (9), 1159-1161.

9) Colby, E.; Lum, G.; Plettner, T.; Spencer, J. Gamma radiation studies on optical materials. *IEEE Trans. Nucl. Sci.* **2002**, 49 (6), 2857-2867.

10) Patel, N. S.; Monmeyran, C.; Agarwal, A.; Kimerling, L. C. Point defect states in Sb-doped germanium. *J. Appl. Phys.* **2015**, 118 (15), 155702-20.

11) Grillanda, S.; Singh, V.; Raghunathan, V.; Morichetti, F.; Melloni, A.; Kimerling, L.; Agarwal, A. M. Gamma radiation effects on silicon photonic waveguides. *Optics Letters* **2016**, in press.

12) Bhandaru, S.; Hu, S.; Fleetwood, D. M.; Weiss, S. M. Total ionizing dose effects on silicon ring resonators. *IEEE Trans. Nucl. Sci* **2015**, 62 (1), 323-328.

13) Storey, S.; Boeuf, F.; Baudot, C.; Detraz, S.; Fedeli, J. M.; Marris-Morini, D.; Olantera, L.; Pezzullo, G.; Sigaud, C.; Soos, C.; Troska, J.; Vasey, F.; Vivien, L.; Zeiler, M.; Ziebell, M. Effect of radiation on a Mach-Zehnder interferometer silicon modulator for HL-LHC data transmission applications. *IEEE Trans. Nucl. Sci.* **2015**, 62 (1), 329-335.

14) Brasch, V.; Chen, Q. F.; Schiller, S.; Kippenberg, T. J. Radiation hardness of high-Q silicon nitride microresonators for space compatible integrated optics. *Opt. Exp.* **2014**, 22 (25), 30786-30794.

15) Lai, C. C.; Chang, C. Y.; Wei, Y. Y.; Wang, W. S. Study of gamma-irradiation damage in $LiNbO_3$ waveguides. *IEEE Photon. Technol. Lett.* **2007**, 19 (13), 1002-1004.

16) Lai, C. C.; Wei, T. Y.; Chang, C. Y.; Wang, W. S.; Wei, Y. Y. Gamma-ray irradiated polymer optical waveguides. *Appl. Phys. Lett.* **2008**, 92 (2), 02330-3.

17) Borodinov, N.; Giammarco, J.; Patel, N.; Agarwal, A.; O'Donnell, K. R.; Kucera, C. J.; Jacobsohn, L. G.; Luzinov, I. Stability of grafted polymer nanoscale films toward gamma irradiation. *ACS Appl. Mater. Interfaces* **2015**, 7 (34), 19455-19465.

18) Morichetti, F.; Melloni, A., Breda, A.; Canciamilla, A.; Ferrari, C.; Martinelli, M. A reconfigurable architecture for continuously variable optical slow-wave delay lines. *Opt. Express* **2007**, 15 (25), 17273-17282.

19) Ziegler, J. SRIM & TRIM software. http://www.srim.org/.